STRUCTURAL BIOLOGY COMMUNICATIONS

ISSN: 2053-230X
journals.iucr.org/f

Structure of the catalytic domain of Mre11 from *Chaetomium thermophilum*

Florian Ulrich Seifert, Katja Lammens and Karl-Peter Hopfner

Acta Cryst. (2015). F**71**, 752–757

STRUCTURAL BIOLOGY COMMUNICATIONS

ISSN 2053-230X

Structure of the catalytic domain of Mre11 from *Chaetomium thermophilum*

Florian Ulrich Seifert, Katja Lammens and Karl-Peter Hopfner*

Gene Center and Department of Biochemistry, Ludwig-Maximilians-University Munich, Feodor-Lynen-Strasse 25, 81377 Munich, Germany. *Correspondence e-mail: hopfner@genzentrum.lmu.de

Received 12 March 2015
Accepted 16 April 2015

Edited by N. Sträter, University of Leipzig, Germany

Keywords: Mre11 nuclease; MRN complex.

PDB reference: Mre11 catalytic domain, 4yke

Supporting information: this article has supporting information at journals.iucr.org/f

Together with the Rad50 ATPase, the Mre11 nuclease forms an evolutionarily conserved protein complex that plays a central role in the repair of DNA double-strand breaks (DSBs). Mre11–Rad50 detects and processes DNA ends, and has functions in the tethering as well as the signalling of DSBs. The Mre11 dimer can bind one or two DNA ends or hairpins, and processes DNA endonucleolytically as well as exonucleolytically in the 3′-to-5′ direction. Here, the crystal structure of the Mre11 catalytic domain dimer from *Chaetomium thermophilum* (CtMre11^{CD}) is reported. CtMre11^{CD} crystals diffracted to 2.8 Å resolution and revealed previously undefined features within the dimer interface, in particular fully ordered eukaryote-specific insertion loops that considerably expand the dimer interface. Furthermore, comparison with other eukaryotic Mre11 structures reveals differences in the conformations of the dimer and the capping domain. In summary, the results reported here provide new insights into the architecture of the eukaryotic Mre11 dimer.

1. Introduction

Double-strand breaks (DSBs), which occur through exposure to genotoxic chemicals, ionizing radiation or reactive oxygen species or during replication-fork blockage (Costanzo *et al.*, 2001; Sutherland *et al.*, 2000; Aguilera & Gómez-González, 2008; Cadet *et al.*, 2012; Mehta & Haber, 2014), are one of the most threatening forms of DNA damage. On the other hand, DSBs are enzymatically introduced in a programmed fashion during meiosis and V(D)J or class-switch recombination during immunoglobulin development (Lam & Keeney, 2014; Gapud & Sleckman, 2011; Xu *et al.*, 2012). To prevent chromosomal rearrangements and genome instability, organisms in all kingdoms of life have developed different DSB-repair pathways (Hanahan & Weinberg, 2011; Myung, Chen *et al.*, 2001; Myung, Datta *et al.*, 2001).

DSBs are repaired by principal pathways such as non-homologous end joining (NHEJ) and homology-directed repair or homologous recombination (HR), or alternative pathways such as microhomology-mediated end joining (MMEJ) (Chiruvella *et al.*, 2013; Chapman *et al.*, 2012). In eukaryotes, the Mre11–Rad50–Nbs1 (MRN) complex plays a key role in the early steps of DSB repair, and its function in the initial detection and processing of DNA ends is important for the choice between resection-dependent (HR, MMEJ) and resection-independent (NHEJ) pathways (Lisby *et al.*, 2004; Truong *et al.*, 2013; Chiruvella *et al.*, 2013; Shibata *et al.*, 2014). MRN consists of a dimer of Mre11, two Rad50s and, in eukaryotes, Nbs1 (Lammens *et al.*, 2011; Schiller *et al.*, 2012; Möckel *et al.*, 2012; Lim *et al.*, 2011; Arthur *et al.*, 2004; Das *et al.*, 2010; Limbo *et al.*, 2012). The Mre11 nuclease forms the enzymatically active centre of the complex. *In vitro*, Mre11 is

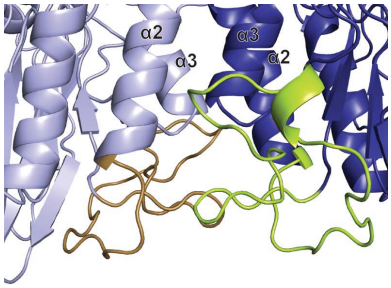

Table 1
Crystallization.

Method	Hanging-drop vapour diffusion
Plate type	24-well plates (Crystalgen SuperClear Plates, pregreased; Jena Bioscience)
Temperature (K)	292
Protein concentration (mg ml^{-1})	7.0
Buffer composition of protein solution	200 m*M* NaCl, 25 m*M* Tris pH 8.0
Composition of reservoir solution	200 m*M* ammonium citrate tribasic pH 6.8–7.0, 18%(*w*/*v*) PEG 3350
Volume and ratio of drop	3 µl; 2:1 protein:reservoir
Volume of reservoir (µl)	500

able to process DNA exonucleolytically in the 3′-to-5′ direction and cuts ssDNA endonucleolytically (Trujillo *et al.*, 1998; Hopfner *et al.*, 2001). To date, Mre11 has been found as a dimer in all available crystal structures. Although comparison of these structures reveals a highly conserved overall shape of the protein, consisting of an N-terminal phosphodiesterase domain followed by a capping domain, the dimer angle between the Mre11 protomers can adopt remarkably different conformations (Schiller *et al.*, 2014). In eukaryotes, the dimer angle is stabilized by latching loops that provide a critical interaction site for Nbs1 with Mre11 (Schiller *et al.*, 2012; Park *et al.*, 2011). However, a substantial portion of the functionally important, eukaryote-specific latching loops remained disordered in previously determined structures (Schiller *et al.*, 2012; Park *et al.*, 2011). Here, we present the crystal structure of the Mre11 catalytic domain dimer from the thermophilic eukaryote *Chaetomium thermophilum* (CtMre11^{CD}) at 2.8 Å resolution. We find interpretable electron density for the entire latching loops, revealing an unexpected expansion of the Mre11 dimer interface by this functionally critical region.

2. Materials and methods

2.1. Protein expression and purification

For co-expression, open reading frames for the components of the MRN head complex (MRN^{HC}) were cloned into two different expression vectors. The Mre11 sequence coding for amino acids 1–537 was cloned into pET-21b vector (Novagen) with NdeI and NotI, and a C-terminal His_6 tag from the vector was fused to the polypeptide chain. Three constructs coding for the Rad50 N- and C-termini (amino acids 1–224 and 1103–1315, respectively) as well as Nbs1 (amino acids 565–714) were first cloned into a modified polycistronic pET-29 vector with NdeI/NotI and then combined with AarI/AscI into a single vector. After co-transformation and induction at an OD_{600} of 0.8 with IPTG (0.3 m*M* final concentration), expression in *Escherichia coli* Rosetta (DE3) cells took place overnight at 18° C. After cell resuspension in lysis buffer (300 m*M* NaCl, 25 m*M* Tris pH 8.0) plus 10 m*M* imidazole and disruption by sonication, cell debris was removed by centrifugation. The supernatant was incubated with nickel–NTA (Qiagen) for 2 h at 7°C. The nickel–NTA column was washed with 10 column volumes (CVs) of lysis buffer and 5 CVs each of lysis buffer containing 20 and then 50 m*M* imidazole. The protein complex was eluted with lysis buffer containing 250 m*M* imidazole. Subsequently, size-exclusion chromatography (Superdex 200 26/60, GE Healthcare) was performed (buffer: 200 m*M* NaCl, 25 m*M* Tris pH 8.0); the purified protein was concentrated to 7.0 mg ml^{-1} and aliquots were frozen in liquid nitrogen.

Table 2
Data collection and processing.

Values in parentheses are for the outer shell.

Diffraction source	Beamline X06SA, SLS
Wavelength (Å)	0.979600
Temperature (K)	199.4
Detector	MAR Mosaic 225 CCD
Crystal-to-detector distance (mm)	270.00
Rotation range per image (°)	1.0
Total rotation range (°)	180
Exposure time per image (s)	1.0
Space group	$P2_12_12_1$
a, *b*, *c* (Å)	56.7, 56.6, 304.6
α, β, γ (°)	90, 90, 90
Mosaicity (°)	0.245
Resolution range (Å)	50.00–2.78 (2.95–2.78)
Total No. of reflections	168505 (22412)
No. of unique reflections	25153 (3657)
Completeness (%)	98.1 (89.5)
Multiplicity	6.7 (6.13)
$\langle I/\sigma(I)\rangle$	11.18 (1.81)
$CC_{1/2}$	99.6 (74.5)
R_{meas}	0.136 (0.962)
Overall *B* factor from Wilson plot (Å^2)	65.1

2.2. Crystallization

Crystallization trials with the MRN^{HC} protein were performed by hanging-drop vapour diffusion (Table 1). Small plate-shaped crystals appeared after three months, and after a further month these were transferred into reservoir solution containing 10%(*v*/*v*) 2,3-butanediol for cryoprotection. The crystals were flash-cooled and stored in liquid nitrogen.

2.3. Data collection and processing

Data were collected on the X06SA beamline at the Swiss Light Source (SLS), Villigen, Switzerland. The data were indexed and integrated with *XDS* (Kabsch, 2010*a*,*b*). Data-collection statistics are shown in Table 2.

2.4. Structure solution and refinement

The *L*-test from *POINTLESS* indicated the presence of twinning and further analysis with *phenix.xtriage* identified the twin operator as $k, h, -l$ (Adams *et al.*, 2010; Winn *et al.*, 2011; Evans, 2006, 2011). The structure of the *C. thermophilum* Mre11 catalytic domain (CtMre11^{CD}; amino acids 4–412) was solved by molecular replacement with *Phaser* (McCoy *et al.*, 2007). The search model was the structure of monomeric *Schizosaccharomyces pombe* Mre11 (PDB entry 4fbq; Schiller *et al.*, 2012), which was co-crystallized with an Nbs1 construct. The structure was refined with *PHENIX*, accounting for twinning (Adams *et al.*, 2010), in combination with manual model building using *Coot* (Emsley & Cowtan, 2004; Emsley *et al.*, 2010). An initial round of rigid-body refinement was followed by restrained refinement with TLS refinement. The

$F_o - F_c$ map revealed density for two manganese ions in the active site, and water molecules were added manually. Structure factors and atomic coordinates of CtMre11^{CD} have been deposited in the Protein Data Bank with accession code 4yke and refinement statistics are reported in Table 3.

3. Results and discussion

We crystallized the catalytic domain of CtMre11 (CtMre11^{CD}; amino acids 4–412) and determined the structure by molecular replacement using *S. pombe* Mre11 (SpMre11^{CD}) as the search model (PDB entry 4fbq; Schiller *et al.*, 2012). The crystallization screen contained the MRN head complex (MRN^{HC}) and, presumably owing to proteolysis, CtMre11^{CD} crystals formed. CtMre11^{CD} contains an N-terminal nuclease domain, which is characterized by a phosphodiesterase motif, and a C-terminal capping domain (amino acids 300–412; Fig. 1*a*). The asymmetric unit consists of two Mre11 protomers that together form the characteristic, previously observed Mre11 dimer mediated by interactions between α-helices α2 and α3 (Hopfner *et al.*, 2001; Schiller *et al.*, 2012; Fig. 1 and Supplementary Fig. S1). The interface between these two helices consists of mainly hydrophobic residues: Tyr70, Met73, Leu139 and Val142. The dimer interface is extended by Arg66, which forms hydrogen bonds to Asn62, Ser129 and Leu134 from the other protomer (Fig. 2*a*). The two manganese ions that are present in the nuclease domains of both CtMre11^{CD} protomers are coordinated in a similar fashion by the absolutely conserved residues Asp17, His19, Asp57, Asn124, His213, His241 and His243 (Schiller *et al.*, 2012; Fig. 2*b*).

Table 3
Structure refinement.

Values in parentheses are for the outer shell.

Resolution range (Å)	49.52–2.78 (2.89–2.78)
Completeness (%)	98.2
No. of reflections, working set	25153 (2253)
No. of reflections, test set	1251 (110)
Final R_{work} (%)	19.8 (30.8)
Final R_{free} (%)	23.1 (40.1)
No. of non-H atoms	
Protein	6548
Manganese	4
Water	60
Total	6612
R.m.s. deviations	
Bonds (Å)	0.003
Angles (°)	0.683
Average *B* factors (Å^2)	
Protein	83.9
Manganese	60.0
Water	45.0
Ramachandran plot	
Favoured regions (%)	96
Additionally allowed (%)	4
Outliers (%)	0

Structural comparison of the individual Mre11 protomers of CtMre11^{CD} with *Homo sapiens* Mre11^{CD} (HsMre11^{CD}) and SpMre11^{CD} reveals that they have similar structures, consistent with their high sequence identities of 46 and 61%, respectively (Schiller *et al.*, 2012; Park *et al.*, 2011; Sievers *et al.*, 2011; Goujon *et al.*, 2010). CtMre11^{CD} largely adopts the conformation of SpMre11^{CD}, but is even more compact than either Nbs1-bound or unbound SpMre11^{CD} owing to an

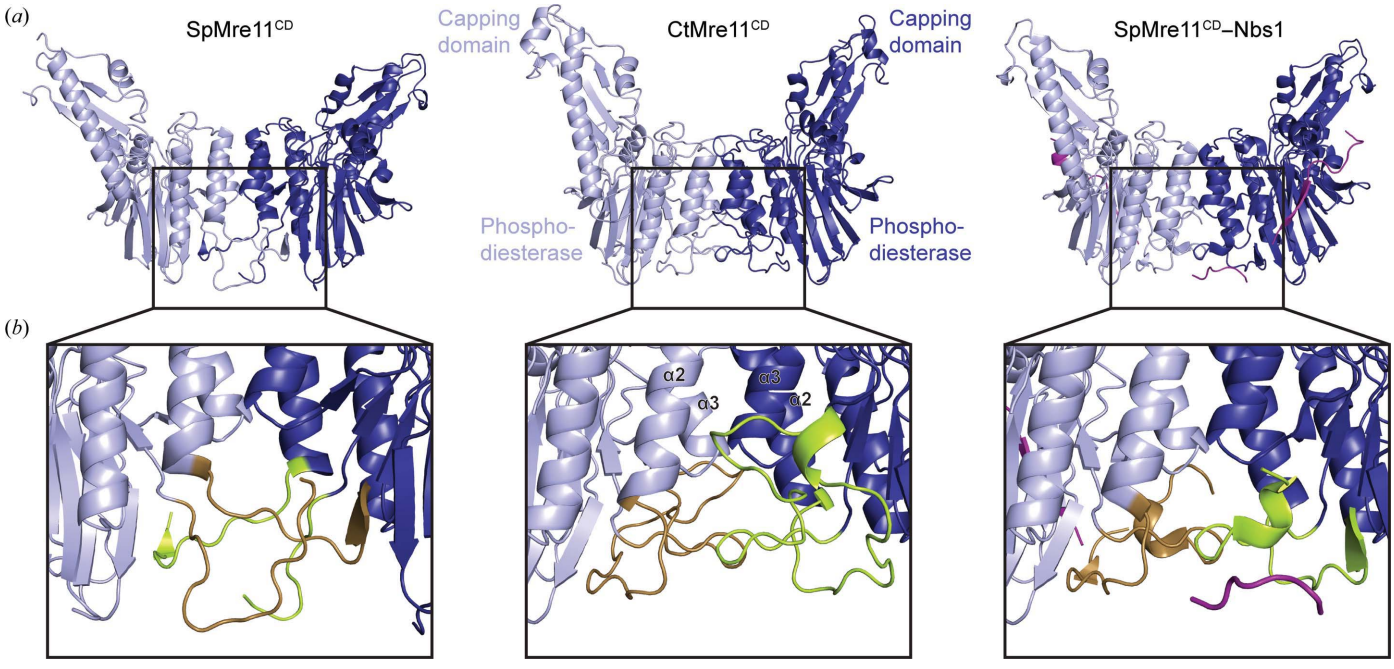

Figure 1
Crystal structure of CtMre11^{CD} and comparison with Nbs1-bound and unbound SpMre11^{CD} structures (SpMre11^{CD} and SpMre11^{CD}–Nbs1, respectively). (*a*) Structures of the dimer of the catalytic domains of SpMre11^{CD}, CtMre11^{CD} and SpMre11^{CD} in complex with the Nbs1 peptide (purple; SpMre11^{CD}–Nbs1; PDB entries 4fcx, 4yke and 4fbw, respectively). The models are displayed in ribbon representation. Mre11 protomers are highlighted in light and deep blue. (*b*) Details of the Mre11 dimer interface and the eukaryotic insertion loops (lime and brown). The conformation of the CtMre11^{CD} insertion loops is similar to the conformation of the loops in the SpMre11^{CD}–Nbs1 structure.

approximately 5 Å movement of the capping domain towards the nuclease active site (Fig. 2*c*). In contrast, the conformation of the Mre11^{CD} dimer displays greater variation between the eukaryotic Mre11 structures. CtMre11^{CD} and SpMre11^{CD} adopt similar conformations yet differ with respect to the human Mre11^{CD} dimer, in which a significantly different interface between the two nuclease domains is stabilized by a disulfide bond. This disulfide bond is absent in the *S. pombe* structures and the presented CtMre11 structure (Park *et al.*, 2011; Schiller *et al.*, 2012).

Interestingly, comparison with SpMre11^{CD} and the SpMre11^{CD}–Nbs1 complex reveals that CtMre11^{CD} has fully ordered insertion loops even in the absence of Nbs1, and we are now able to model the entire eukaryote-specific loop insertion that plays a critical role in the interaction with Nbs1 and in damage signalling (Figs. 1 and 2*d*). In the case of

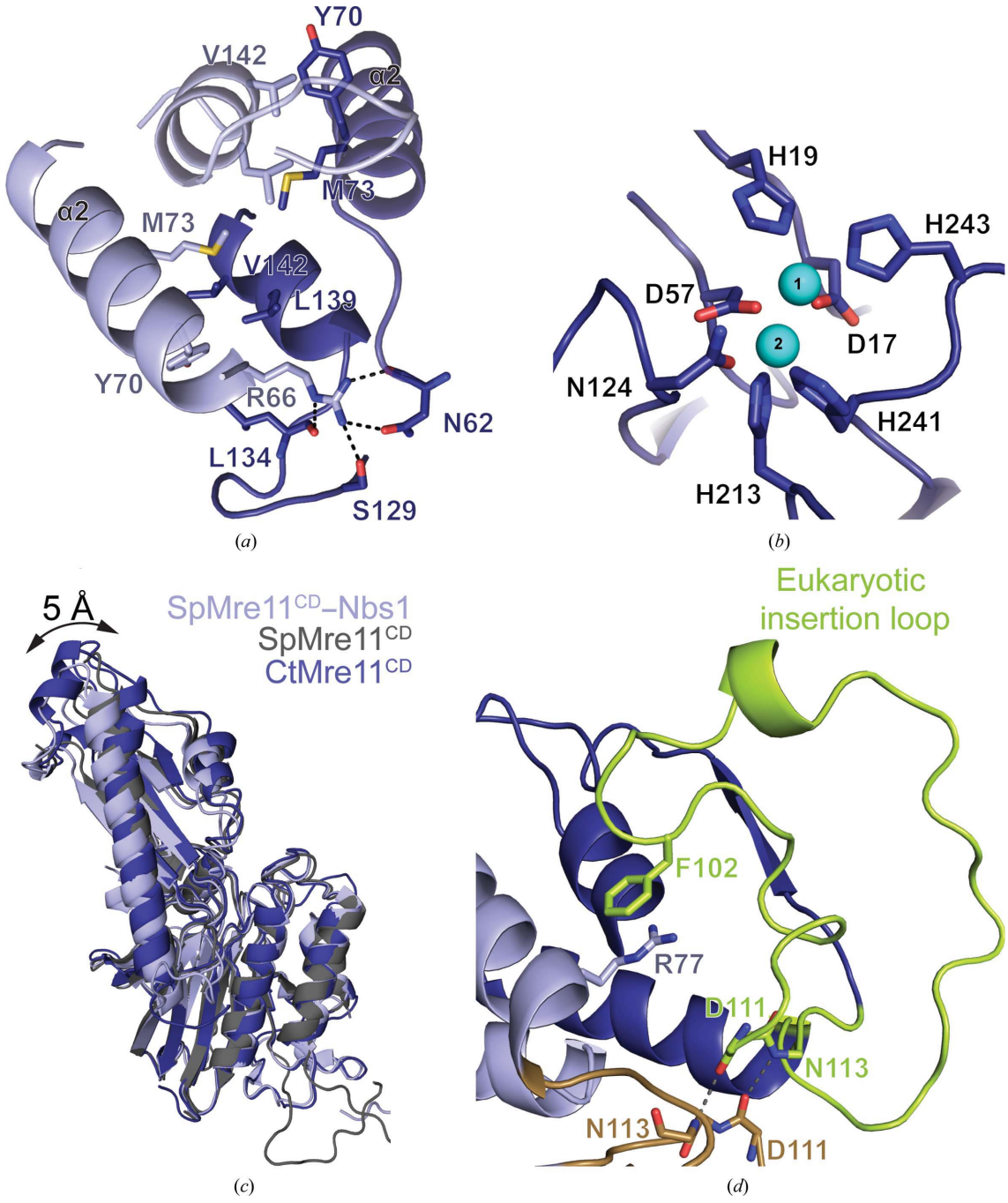

Figure 2
Details of the Mre11^{CD} crystal structure from *C. thermophilum*. (*a*) Detailed view of the CtMre11^{CD} dimer interface consisting of α-helices α2 and α3 from each protomer. (*b*) CtMre11^{CD} nuclease active site with two coordinated manganese ions (cyan). (*c*) Overlay of SpMre11^{CD} (grey), SpMre11^{CD}–Nbs1 (light blue) and CtMre11^{CD} (deep blue) by alignment of the nuclease domains onto the nuclease domain of CtMre11^{CD} indicates the movement of the capping domain by up to 5 Å. (*d*) Fully modelled eukaryotic insertion loop (lime and brown). The interaction between Arg77 and Phe102 is highlighted. Selected residues are depicted as colour-coded sticks and annotated. Hydrogen bonds in (*a*) and (*d*) are highlighted as dashed lines.

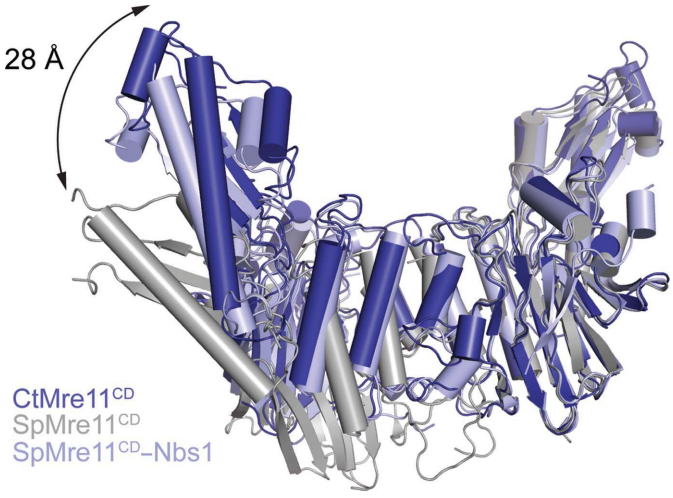

Figure 3
Overlay of CtMre11^{CD}, SpMre11^{CD} and SpMre11^{CD}–Nbs1. Structures of SpMre11^{CD} (grey) and SpMre11^{CD}–Nbs1 (light blue) dimers are aligned *via* one of the two CtMre11^{CD} (dark blue) protomers to show the variability of the dimer interface and dimer angle. The distance between the capping domains of CtMre11^{CD} and SpMre11^{CD} reaches 28 Å.

SpMre11^{CD}, Nbs1 binding partially orders the insertion loops, resulting in a more compact Mre11 dimer (Schiller *et al.*, 2012; Fig. 1*b*). Indeed, the dimeric conformation of CtMre11^{CD} with fully ordered insertion loops is very similar to that of SpMre11^{CD} bound to Nbs1, but is quite distinct from the more open SpMre11^{CD} dimer conformation in the absence of Nbs1 (Fig. 3). The Nbs1-binding site bridging the SpMre11 dimer is occupied in the presented structure by symmetry-related molecules that may stabilize the insertion loops. This dimeric structure of Mre11 enables each nuclease active site to bind a dsDNA substrate and thus allows the bridging of two DNA ends (Williams *et al.*, 2008). Interestingly, the insertion loops extend the Mre11 dimer interface through reaching across the lateral CtMre11^{CD} dimer interface. Notably, the conserved phenylalanine (Phe102 in *C. thermophilum*) stacks with and stabilizes Arg77, a critical residue in stabilizing the Mre11 dimer interface (Schiller *et al.*, 2012), of the opposing protomer (Fig. 2*d*). As a result, the 1490 Å^2 Mre11–Mre11 interface of CtMre11^{CD} is twice as large as that of Mre11 from the thermophilic archaeon *Pyrococcus furiosus* (Krissinel & Henrick, 2007), in which the insertion loops are absent.

In summary, this structure of CtMre11^{CD} fully defines the eukaryotic insertion loops and shows that these loops expand the Mre11 dimer interface (Hopfner *et al.*, 2001). Furthermore, our results show considerable flexibility not only between the Mre11 protomers but also between the phosphodiesterase domain and the capping domain.

Acknowledgements

We thank Brigitte Kessler for help with cloning and protein purification and Robert Byrne for comments on the manuscript, as well as the staff of the Swiss Light Source, Villigen, Switzerland for technical support. This work was funded by the German Research Council projects GRK1721 and SFB684, the Center for Integrated Protein Sciences Munich and the European Research Council Advanced Grant ATMMACHINE to K-PH.

References

Adams, P. D. *et al.* (2010). *Acta Cryst.* D**66**, 213–221.
Aguilera, A. & Gómez-González, B. (2008). *Nature Rev. Genet.* **9**, 204–217.
Arthur, L. M., Gustausson, K., Hopfner, K.-P., Carson, C. T., Stracker, T. H., Karcher, A., Felton, D., Weitzman, M. D., Tainer, J. & Carney, J. P. (2004). *Nucleic Acids Res.* **32**, 1886–1893.
Cadet, J., Ravanat, J. L., TavernaPorro, M., Menoni, H. & Angelov, D. (2012). *Cancer Lett.* **327**, 5–15.
Chapman, J. R., Taylor, M. R. G. & Boulton, S. J. (2012). *Mol. Cell*, **47**, 497–510.
Chiruvella, K. K., Liang, Z. & Wilson, T. E. (2013). *Cold Spring Harb. Perspect. Biol.* **5**, a012757.
Costanzo, V., Robertson, K., Bibikova, M., Kim, E., Grieco, D., Gottesman, M., Carroll, D. & Gautier, J. (2001). *Mol. Cell*, **8**, 137–147.
Das, D. *et al.* (2010). *J. Mol. Biol.* **397**, 647–663.
Emsley, P. & Cowtan, K. (2004). *Acta Cryst.* D**60**, 2126–2132.
Emsley, P., Lohkamp, B., Scott, W. G. & Cowtan, K. (2010). *Acta Cryst.* D**66**, 486–501.
Evans, P. (2006). *Acta Cryst.* D**62**, 72–82.
Evans, P. R. (2011). *Acta Cryst.* D**67**, 282–292.
Gapud, E. J. & Sleckman, B. P. (2011). *Cell Cycle*, **10**, 1928–1935.
Goujon, M., McWilliam, H., Li, W., Valentin, F., Squizzato, S., Paern, J. & Lopez, R. (2010). *Nucleic Acids Res.* **38**, W695–W699.
Hanahan, D. & Weinberg, R. A. (2011). *Cell*, **144**, 646–674.
Hopfner, K. P., Karcher, A., Craig, L., Woo, T. T., Carney, J. P. & Tainer, J. A. (2001). *Cell*, **105**, 473–485.
Kabsch, W. (2010*a*). *Acta Cryst.* D**66**, 125–132.
Kabsch, W. (2010*b*). *Acta Cryst.* D**66**, 133–144.
Krissinel, E. & Henrick, K. (2007). *J. Mol. Biol.* **372**, 774–797.
Lam, I. & Keeney, S. (2014). *Cold Spring Harb. Perspect. Biol.* **7**, a016634.
Lammens, K., Bemeleit, D. J., Möckel, C., Clausing, E., Schele, A., Hartung, S., Schiller, C. B., Lucas, M., Angermüller, C., Söding, J., Strässer, K. & Hopfner, K. P. (2011). *Cell*, **145**, 54–66.
Lim, H. S., Kim, J. S., Park, Y. B., Gwon, G. H. & Cho, Y. (2011). *Genes Dev.* **25**, 1091–1104.
Limbo, O., Moiani, D., Kertokalio, A., Wyman, C., Tainer, J. A. & Russell, P. (2012). *Nucleic Acids Res.* **40**, 11435–11449.
Lisby, M., Barlow, J. H., Burgess, R. C. & Rothstein, R. (2004). *Cell*, **118**, 699–713.
McCoy, A. J., Grosse-Kunstleve, R. W., Adams, P. D., Winn, M. D., Storoni, L. C. & Read, R. J. (2007). *J. Appl. Cryst.* **40**, 658–674.
Mehta, A. & Haber, J. E. (2014). *Cold Spring Harb. Perspect. Biol.* **6**, a016428.
Möckel, C., Lammens, K., Schele, A. & Hopfner, K.-P. (2012). *Nucleic Acids Res.* **40**, 914–927.
Myung, K., Chen, C. & Kolodner, R. D. (2001). *Nature (London)*, **411**, 1073–1076.
Myung, K., Datta, A. & Kolodner, R. D. (2001). *Cell*, **104**, 397–408.
Park, Y. B., Chae, J., Kim, Y. C. & Cho, Y. (2011). *Structure*, **19**, 1591–1602.
Schiller, C. B., Lammens, K., Guerini, I., Coordes, B., Feldmann, H., Schlauderer, F., Möckel, C., Schele, A., Strässer, K., Jackson, S. P. & Hopfner, K.-P. (2012). *Nature Struct. Mol. Biol.* **19**, 693–700.
Schiller, C. B., Seifert, F. U., Linke-Winnebeck, C. & Hopfner, K.-P. (2014). *Cold Spring Harb. Perspect. Biol.* **6**, a017962.
Shibata, A. *et al.* (2014). *Mol. Cell*, **53**, 7–18.
Sievers, F., Wilm, A., Dineen, D., Gibson, T. J., Karplus, K., Li, W., Lopez, R., McWilliam, H., Remmert, M., Söding, J., Thompson, J. D. & Higgins, D. G. (2011). *Mol. Syst. Biol.* **7**, 539.
Sutherland, B. M., Bennett, P. V., Sidorkina, O. & Laval, J. (2000). *Proc. Natl Acad. Sci. USA*, **97**, 103–108.

Trujillo, K. M., Yuan, S.-S. F., Lee, E.-Y. P. & Sung, P. (1998). *J. Biol. Chem.* **273**, 21447–21450.
Truong, L. N., Li, Y., Shi, L. Z., Hwang, P. Y.-H., He, J., Wang, H., Razavian, N., Berns, M. W. & Wu, X. (2013). *Proc. Natl Acad. Sci. USA*, **110**, 7720–7725.
Williams, R. S., Moncalian, G., Williams, J. S., Yamada, Y., Limbo, O., Shin, D. S., Groocock, L. M., Cahill, D., Hitomi, C., Guenther, G., Moiani, D., Carney, J. P., Russell, P. & Tainer, J. A. (2008). *Cell*, **135**, 97–109.
Winn, M. D. *et al.* (2011). *Acta Cryst.* D**67**, 235–242.
Xu, Z., Zan, H., Pone, E. J., Mai, T. & Casali, P. (2012). *Nature Rev. Immunol.* **12**, 517–531.